18th International Conference
ENGINEERING MECHANICS 2012
Svratka, Czech Republic, May 14 – 17, 2012

pp. 191–201
Paper #87

COMPUTATIONAL STUDY OF SLUDGE PUMP DESIGN WITH VORTEX IMPELLER

M. Červinka*

Abstract: *This paper presents a computational study of sludge pump design with vortex impeller. It contains two design variants of vortex impeller, which is supported by CFD calculations in ANSYS Fluent. By modeling the problem in Fluent, it has been verified that such impellers could be fitted into the existing spiral casing with channel impeller. It was verified that the original operating parameters were maintained. Results of these design solutions and evaluation of effect of some construction modifications on the pump characteristics have been shown.*

Keywords: ***Sludge pump, vortex impeller, characteristics, design, Computational Fluid Dynamic.***

1. Introduction

Sludge pumps are used in many different branches of industry. We can find them in wastewater treatment plants, industry, home, etc. These pumps are very often used for polluted water pumping with abrasive particles. For this reason, these pumps can differ in construction, shape or used materials from classical hydrodynamic pumps. This paper describes a design of vortex impeller which can be fitted into existing spiral casing of original sludge pump with channel impeller. In the following chapters, this design will be introduced. It was proposed using the original operating parameters and the impeller is based on the principle of vortex impeller with commercial name TURO. These impellers are patented by Swiss company Egger. The second design variant of impeller is based on the vortex impeller which is called SuperVortex and is made by Danish company Grunfos. Models were created for both impellers and the CFD (Computational Fluid Dynamic) computations for both design variants were made to assess suitability of use. For solution and subsequent evaluation of this problem we used the values obtained from CFD calculations.

2. TURO impeller

The Turo impeller has lots of advantages. First, it is placed in a different position compared to the channel impellers; thus the large vortex under impeller is created. These impellers are used to pump polluted water with high content of abrasive particles therefore only approximately 15% of impurities get into contact with the impeller. For this reason there is less danger of abrasive wear than with classical channel impellers. Next advantage is that these impellers usually have a stable characteristic and in most cases only very low radial force acts on the impeller. Another advantage is a very simple construction. Efficiency of these types of impellers is between $\eta = (40 \div 55)$ %. A Working principle of this pump is shown in fig.1 and a typical pump with the Turo impeller is shown in fig. 2.

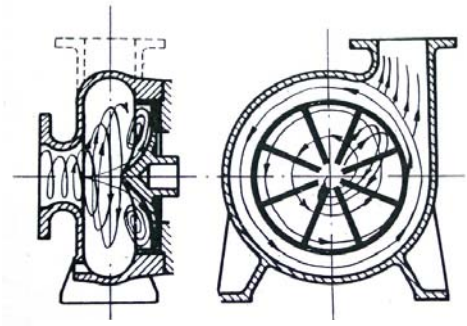

Fig. 1: Working principle of the Turo pump

Fig. 2: Typical pump with Turo impeller (Egger, 2008)

*Ing.Martin Červinka: Victor Kaplan's Department of Fluid Engineering, Institute of Energy, Brno University of Technology, Faculty of Mechanical Engineering, Technická 2896/2; 616 69, Brno; CZ, e-mail: y100967@stud.fme.vutbr.cz

3. Design of impellers

As mentioned above two models of impellers were created. At first the Turo impeller model was created. Basic equations described in (Feranec, 200?) were used to design this impeller. Original parameters of the pump are shown in Tab. 1. These parameters and known dimensions of spiral casing were used and main dimensions of Turo impeller were designed. The model of Turo impeller can be seen in fig. 3. Secondly, the other impeller model was created by cranking the vanes from the Turo impeller and by creating the so called spur. For this reason this impeller will be called "Turo with spur" and it can be seen in fig. 4.

3.1. Main dimensions of impeller

According to basic equations, main dimensions were created. In the following chapter, basic equations and calculated main dimensions can be seen.

Tab. 1: Original operating parameters.

Title	***Sign***	***Value***	***Unit***
Flow rate	Q	35.8	[l/s]
Head	H	21.5	[m]
Density	ρ	1050	[kg/m^3]
Speed	n	1450	[1/min]
Power	P	15	[kW]
Number of blades	z	8	[-]
Inlet, outlet angle of blade	β_1 , β_2	90	[°]

Diameter of impeller D_2

$$\Psi=\frac{g.H}{\frac{u_2^2}{2}}=\frac{2.g.H}{u_2^2} \tag{1}$$

$$u_2^2=\frac{2.g.H}{\Psi} \tag{2}$$

$$u_2=\sqrt{\frac{2.g.H}{\Psi}} \tag{3}$$

$$u_2=2\pi n.R_2=\sqrt{2.g}.\sqrt{\frac{H}{\Psi}} \tag{4}$$

$$D_2=84{,}8.\frac{1}{n}.\sqrt{\frac{H}{\Psi}}=84{,}8.\frac{1}{1450}.\sqrt{\frac{21{,}5}{1{,}17}}=\mathbf{0,\ 2507}[\mathrm{m}] \tag{5}$$

According to equations (1) – (4), we can obtain a final equation (5) for the impeller diameter. Based on this the value of diameter was chosen as $\boldsymbol{D_2 = 0{,}25\ m}$

Impeller width b_2

$$\frac{b_4}{b_2} \cong 3 \tag{6}$$

$$b_2 = \frac{b_4}{3} = \frac{0{,}08}{3} = 0{,}026666 \Rightarrow 0{,}027 \quad [\mathrm{m}] \tag{7}$$

Or by other equation

$$b_2 = (0{,}25 \div 0{,}3).D_s = 0{,}3.0{,}126 = 0{,}0378 [\mathrm{m}] \tag{8}$$

From results of equations (7) and (8), the value of impeller width was chosen as ***b_2 = 0,03 m***.

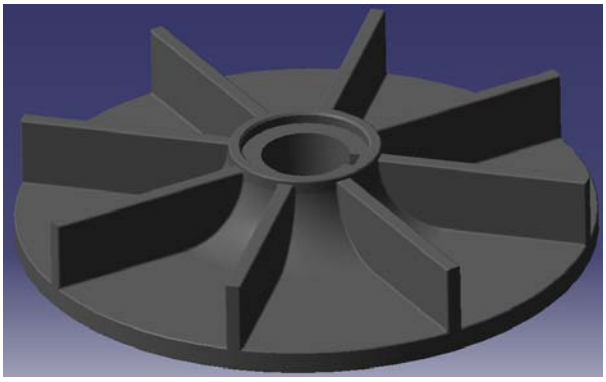

Fig. 3: The Turo impeller model

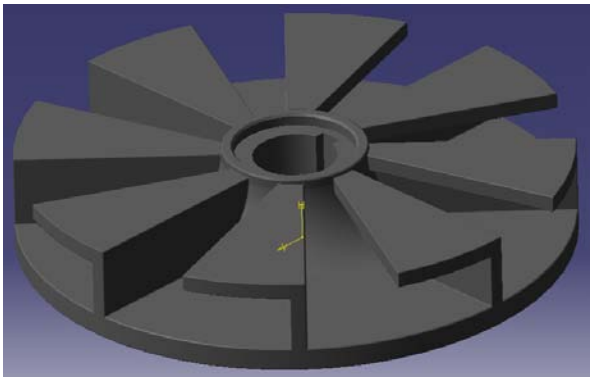

Fig. 4: The Turo with spur impeller model

3.2. Design of CFD model

Geometrical models of both impellers were created in Gambit 2.4.6. The computational mesh contained approximately 6 million hexahedral cells; the worst cell had skewness equal to 0. 7711. The whole model was split into 5 volumes: impeller, space above impeller, spiral casing, suction and displacement. The computation was done in ANSYS Fluent 12. 1 and 2 equation k- ε viscosity model with non – equilibrium wall function was used. A steady calculation with second order upwind was performed. To create all of these characteristics, an overall range of flow rate must be taken into account. Following design points were computed: ***1,25* Q_N*** (45 $l.s^{-1}$); ***Q_N*** (36 $l.s^{-1}$); ***0,75* Q_N*** (27 $l.s^{-1}$); ***0,5* Q_N*** (18 $l.s^{-1}$); ***0,25* Q_N*** (9 $l.s^{-1}$) and finally, last point ***0,1* Q_N*** (3,6 $l.s^{-1}$) for better projection of characteristics at low flow rate was added.

4. Evaluation

4.1. Characteristics of pump

A focus was put on the following characteristics Y – Q, η – Q, P – Q. As stated in (Pochylý et. al., 2009), the Y – Q characteristic should be considered as stable if the following condition of stability is fulfilled across the whole range of the flow rate:

$$\frac{\partial Y}{\partial Q} < 0 \tag{9}$$

The characteristics of pump with Turo impeller are shown in fig. 5, 6, and 7; the characteristic is stable across the whole range of flow rate. The power characteristic has almost a linear shape although there is a slight deviation near the shut-off point due to inaccuracies in the calculation. According to the general theory, the progress of these characteristics can be assessed as correct. At a design optimum we obtained head H = 22,23 m, power P = 13385 W and efficiency η = 58, 4%, which are higher values than original operating parameters.

The characteristics of pump with Turo with spur impeller are in principle the same as Turo. In fig. 5 the relation between specific energy and flow rate can be seen. It is as stable as the Turo impeller characteristic but the decrease of specific energy and related head can be seen. At the design optimum for Turo with spur impeller we obtained head H = 20, 47 m, power P = 12843 W and efficiency η = 56, 1%, i.e. a decrease compared to the original operating parameters. The difference of specific energy between the design variants is shown in fig. 8.

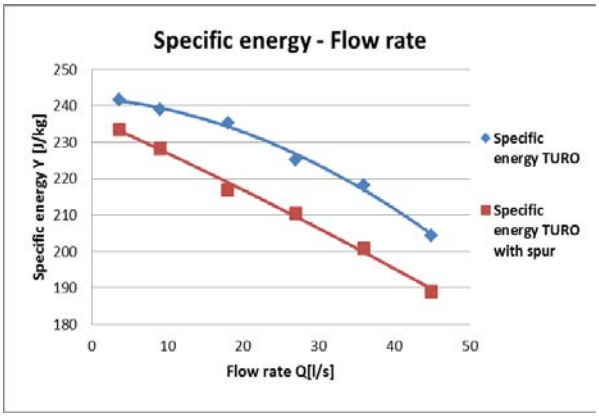

Fig. 5: Y – Q characteristics for both design variants

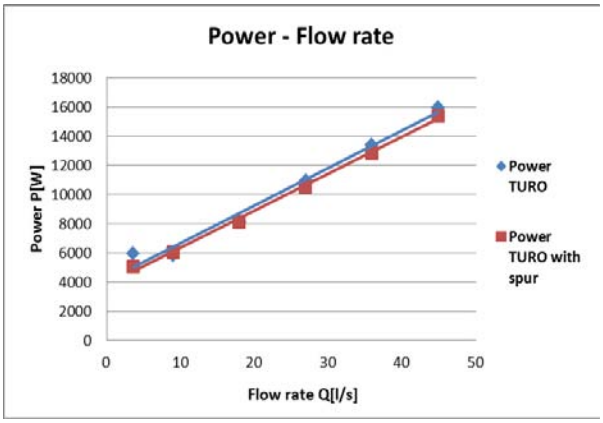

Fig. 6: P – Q characteristics for both design variants

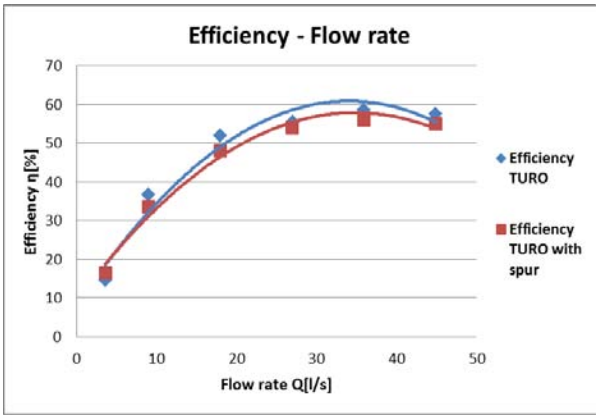

Fig. 7: η – Q characteristics for both design variants

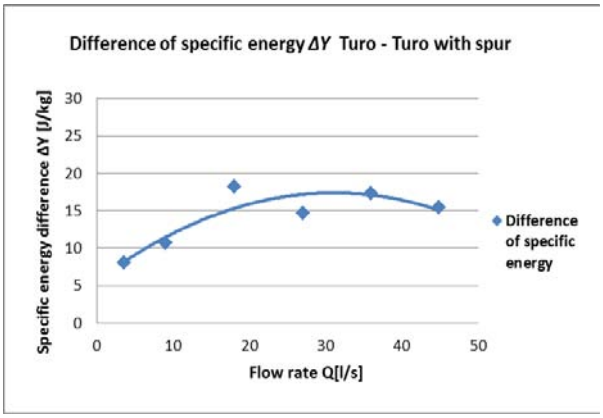

Fig. 8: The difference of specific energy between Turo and Turo with spur impellers

4.2. Specific energy in different volumes of pump

The characteristics of specific energy in dependence on flow rate for different volumes, as introduced in chapter 3.2, are shown in fig. 9 – 12. The characteristics for the Turo impeller are shown in fig. 9, 10 and for the Turo with spur are in fig. 11, 12. For both impeller volumes, characteristics are unstable at a low flow rates, which has a negative impact on total characteristics although they are considered as stable. Both variants have similar shapes of these characteristics for the same volumes.

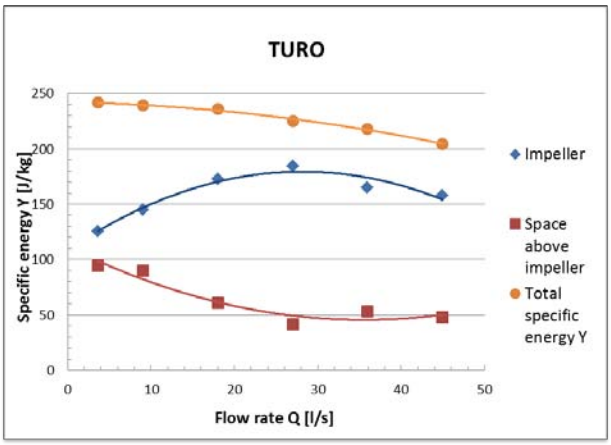

Fig. 9: Y – Q characteristics in specific volumes for Turo impeller

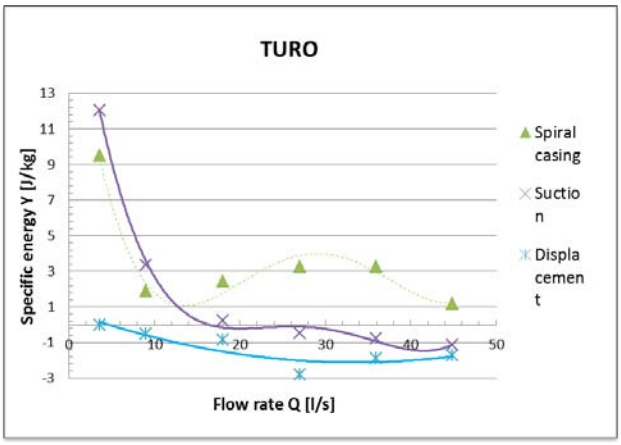

Fig. 10: Y – Q characteristics in specific volumes for Turo impeller

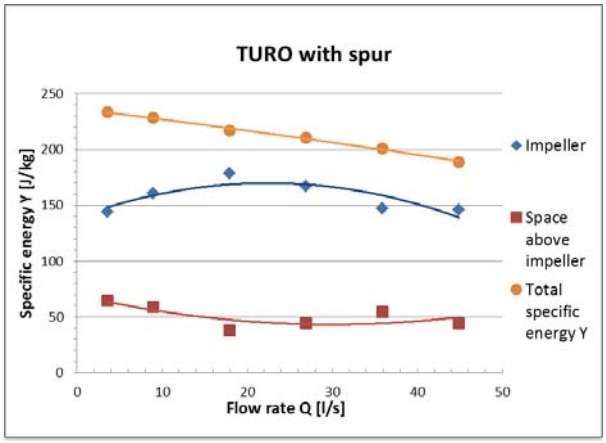

Fig. 11: Y – Q characteristics in specific volumes for Turo with spur impeller

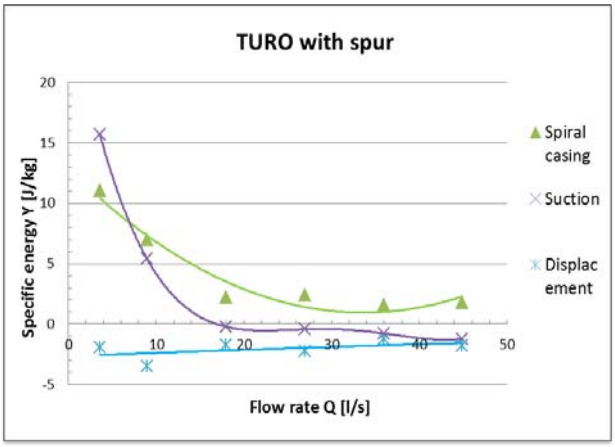

Fig. 12: Y – Q characteristics in specific volumes for Turo with spur impeller

4.3. Axial force

The axial force applied to impellers was obtained, like other values, from CFD computation. The axial force applied on impellers is shown in fig. 13 and the axial force applied only on impeller vanes for both design variants is shown in fig. 14. The axial force is oriented in positive direction of z – axis, i.e. it is negative values are directed into the impeller and the shaft is subjected to a compressive stress. Values of axial force for the Turo with spur are approximately three times larger than for the Turo. This is probably due to larger vanes of the Turo with spur; therefore fluid can act on the impeller by larger force. The axial force is not large for this type of pump; however it can be lowered by using construction adjustment stated in (Gančo, 1999). The best solution for these impellers is compensatory vanes at the back of supporting disk; these vanes can help to minimalize the effect of axial force.

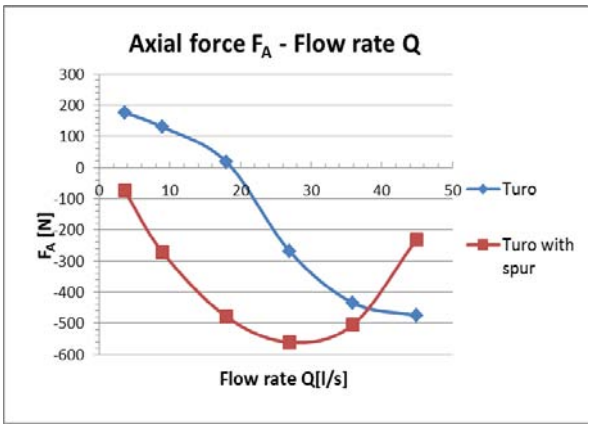

Fig. 13: Axial force on impellers

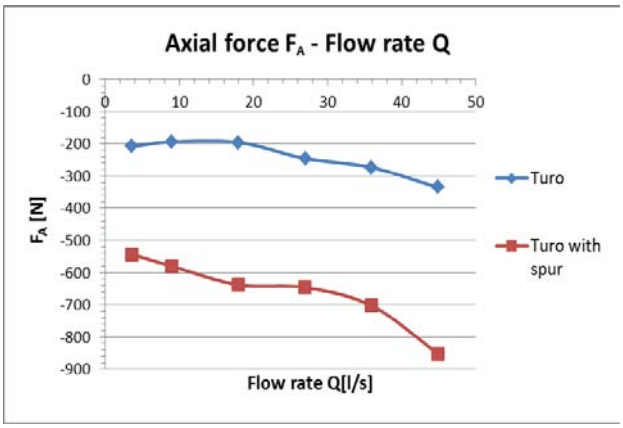

Fig. 14: Axial force on impeller vanes

4.4. Influence of construction modification

The influence of construction modification on pump characteristics was examined in this chapter. Three solutions of gap between the pump casing and the impeller were created. First solution was a conical gap with angle 15°, then a very small cylindrical gap, which was almost like wall behind the impeller and the last solution was a large cylindrical gap between these parts. For better illustration, these gaps are shown in fig. 15. The results from computation and evaluation of influence of each design variant are also shown. After obtaining results from CFD computation, we created all pump characteristics, which are shown in fig. 16, 17 and 18. The first solution (conical gap) shows the best results. The second solution (very small gap) has unstable Y – Q characteristic and the efficiency is lower than for conical gap. The large cylindrical gap has quite similar characteristics as a very small cylindrical gap. According to results presented in this chapter, it can be said that the conical gap with 15° angle achieved the best results and shapes of characteristics. The computation was made only for the Turo impeller.

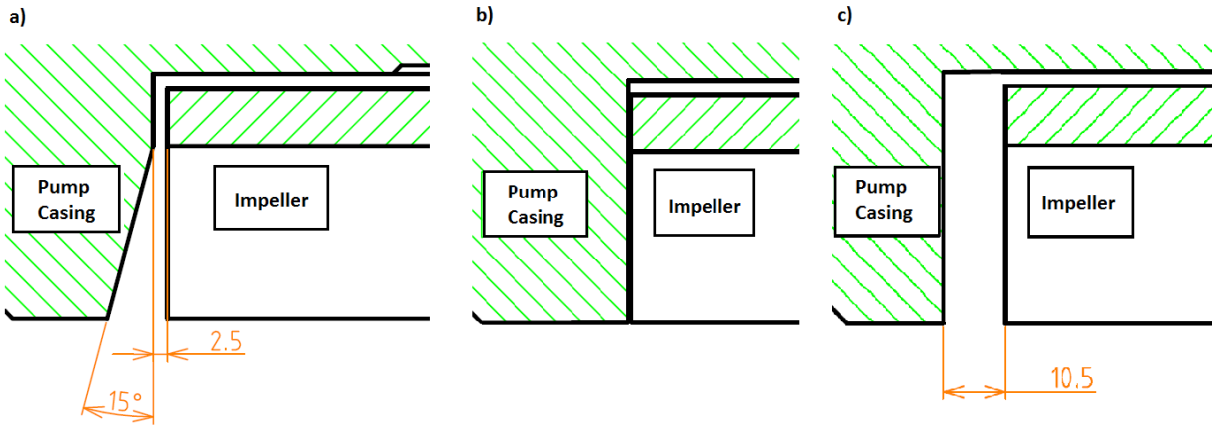

Fig. 15: Types of gaps a) Conical gap; b) Very small cylindrical gap; c) Large cylindrical gap

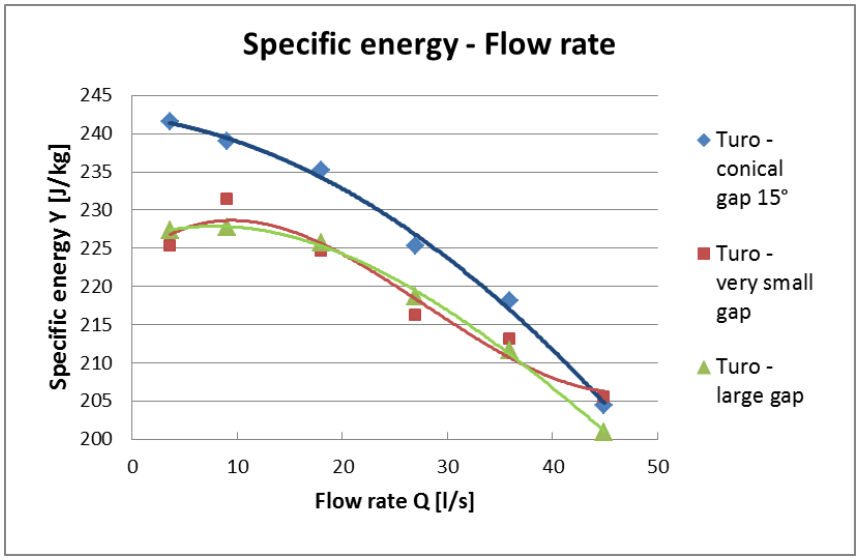

Fig. 16: Y - Q characteristics for different types of gaps

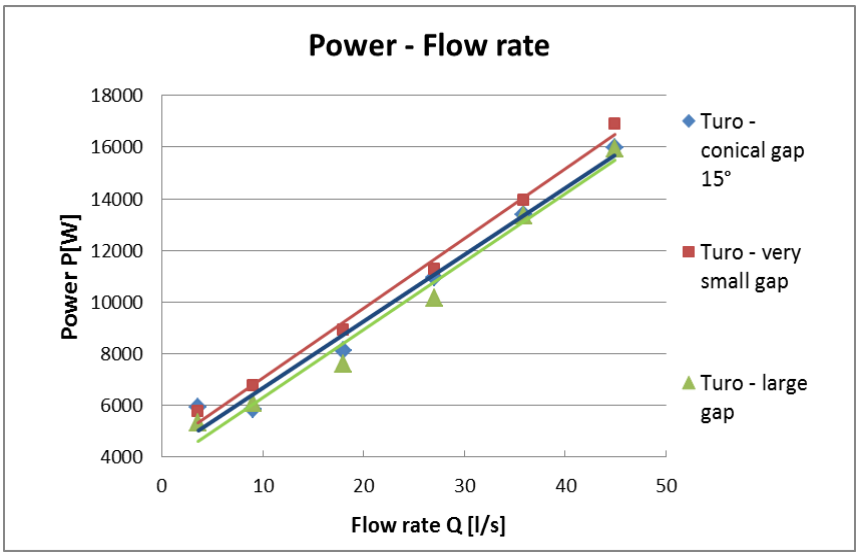

Fig. 17: P - Q characteristics for different types of gaps

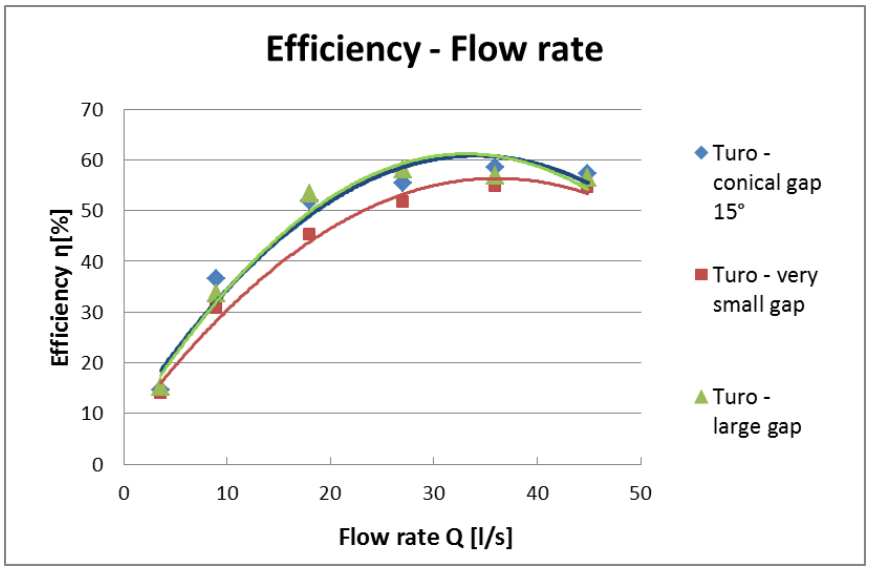

Fig. 18: η – Q characteristics for different types of gaps

4.5. Rotational motion in pump

The model of the whole pump is quite extensive and it is hard to show the behavior of fluid in each part. Velocity vectors and differences between design variants of impeller are shown. The graphic interpretation gives us a possibility to show vortices occurring in our model space, fluid behavior, etc.

4.5.1 Turo impeller

The main focus was put on fluid behavior in the inter vane channel. Velocity vectors are displayed in created cuts, which are shown in fig. 19. Velocity vectors in the impeller space are shown in fig. 20 – 23. Firstly, we considered an inlet to the impeller as it is whole upper face but the figures below show that the fluid began to leave the impeller in the region of larger radius. That is caused by rotation and vortex movement in the impeller. The figures also illustrated that the main vortex in the channel has counter-clockwise direction of rotation (fig. 20, 21) and it is opposite towards the output radius of the impeller (fig. 23). Therefore, the main vortex changes the direction of rotation as the fluid goes through inter blade channel. The magnitude of relative velocities is highest at impeller inlet, i.e. the area of small diameter of the impeller.

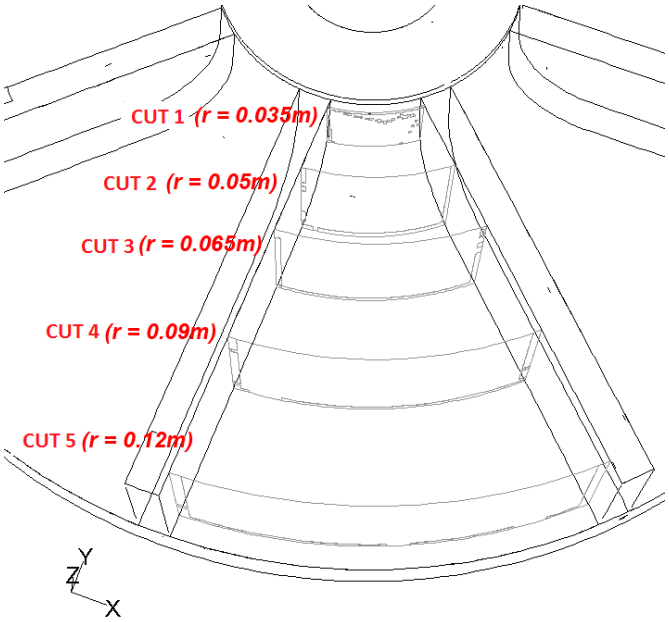

Fig. 19: The cuts in vane channel

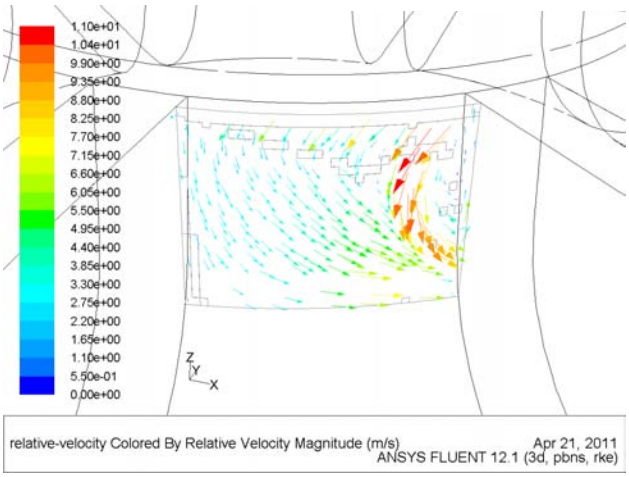

Fig. 20: Relative velocity vectors in cut no.1

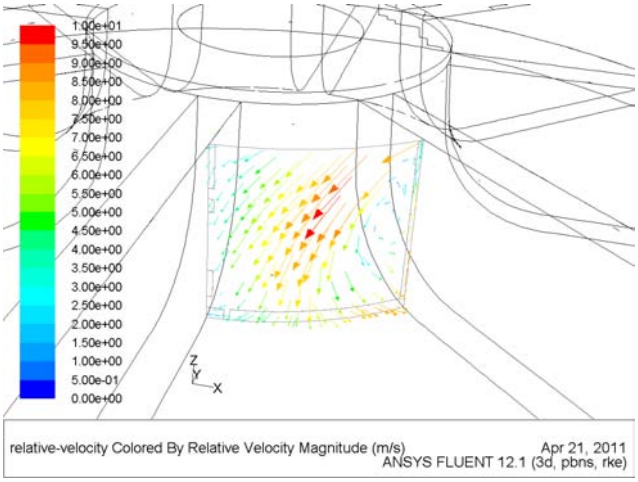

Fig. 21: Relative velocity vectors in cut no.2

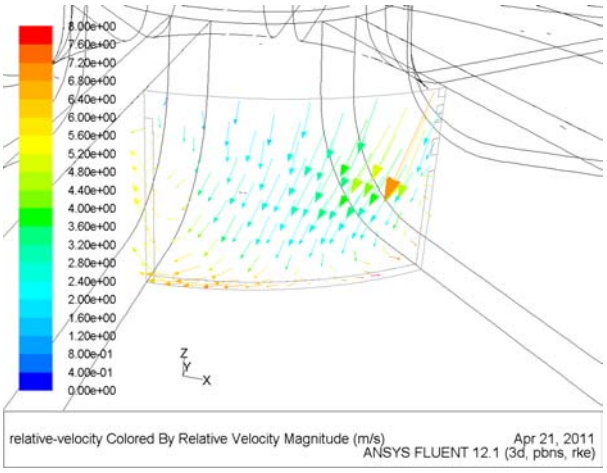

Fig. 22: Relative velocity vectors in cut 3

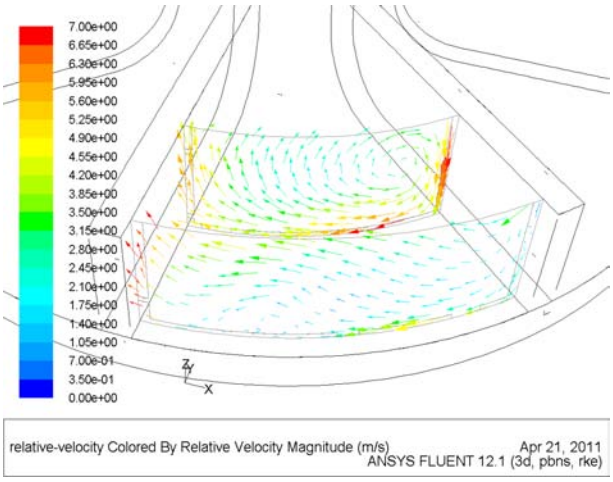

Fig. 23: Relative velocity vectors in cut no.4 and no.5

4.5.2 Turo with spur

The evaluation of the fluid motion in the pump space was also made for the Turo with spur impeller. For this design, velocity vectors in the same cuts are shown and only small differences between both impellers can be seen. The velocity vectors in the cuts are shown in fig. 24 - 27. At the inlet to the inter blade channel of impeller a negative property of the spur can be observed; it shrinks the inlet area such that the fluid cannot flow into the channel as well as for Turo impeller. According to Grundfos Company, which produces SuperVortex impellers, the spur should prevent the occurrence of small disturbing vortices nearby the impeller. Unfortunately, this property cannot be confirmed from achieved results due to limitations of our hardware capacity and this would probably need a finer computational mesh in this area.

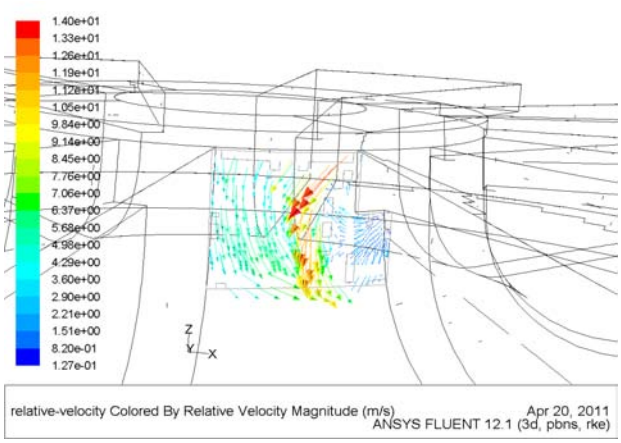

Fig. 24: Relative velocity vectors in cut 1

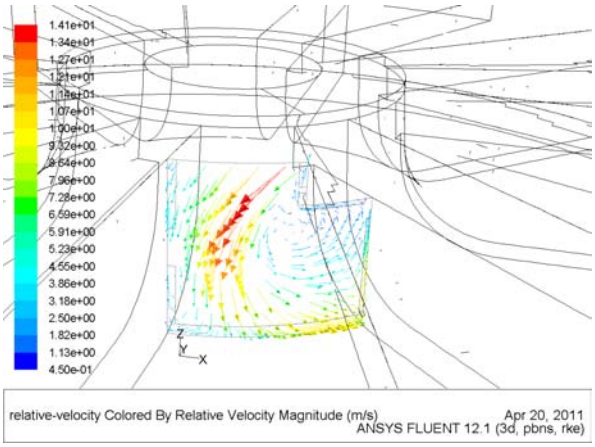

Fig. 25: Relative velocity vectors in cut 2

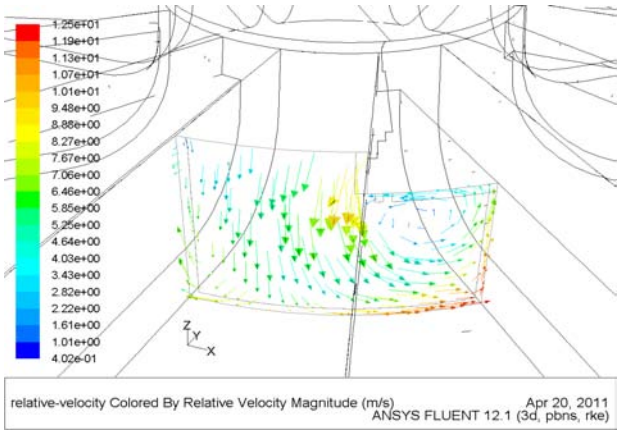

Fig. 26: Relative velocity vectors in cut 3

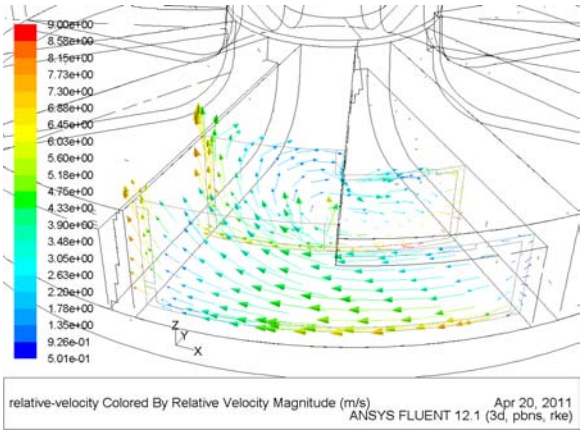

Fig. 27: Relative velocity vectors in cut 4 and 5

The differences at the inlet to impellers can be seen in fig. 28, 29. An interesting property of spur is that it prevents the flow of fluid into the impeller channel. It negatively affects the pump characteristic and it causes a decrease of the characteristic as is described in chapter 4.1.

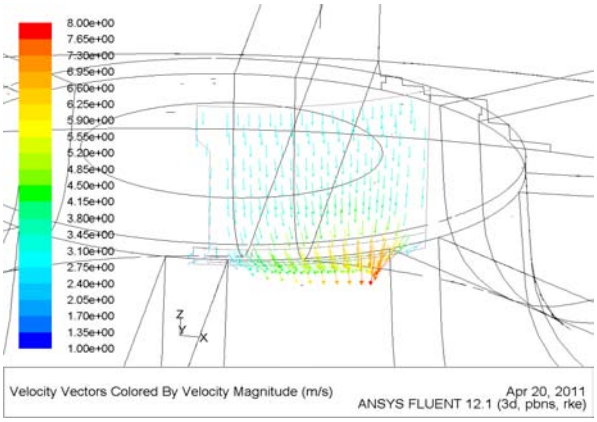

Fig. 28: Relative velocity vectors in inlet section above impeller for the Turo impeller

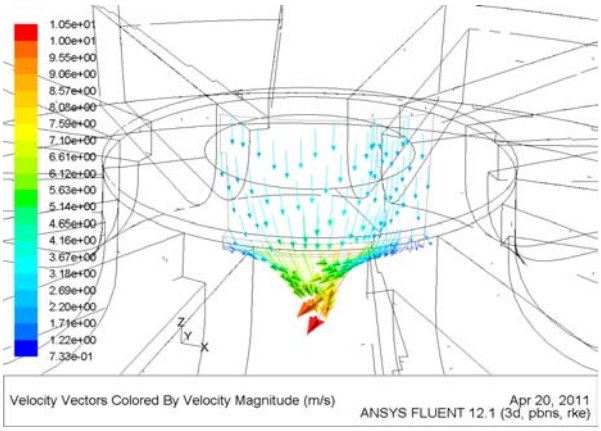

Fig. 29: Relative velocity vectors in inlet section above impeller for the Turo with spur impeller

5. Conclusions

Basic equations for design of Turo impeller are presented in this paper. The Turo impeller fulfilled operating parameters of the original pump. From achieved results it would be possible to change only the impellers with just a slight construction adaptation of the pump casing. The Turo with spur impeller was based on the principle of SuperVortex impeller; a decrease of characteristics values can be seen in this variant. The reason of this decrease follows from the fact that the spur has been designed such that it overlaps a part of the vane channel which caused a partial blockage. To improve this we can design the spur from the middle of the vane so that it would not block the fluid at inlet. We cannot confirm that the spur has a proper function because the results are not as predicative as we needed. The axial force acting on impellers of this type of pumps is not large. Moreover, it can be improved by some construction adjustments as mentioned in chapter 4.3. Both impellers have a stable Y – Q characteristic; this is very important in terms of occurrence of undesired pressure and flow pulsations. Finally, the influence of construction design of some parts of pump casing on pump characteristics was examined. This paper has shown three different solutions of a gap between the impeller and the pump casing. From results shown in chapter 4.4, it can be seen to what extent the

characteristic can be influenced by this change. There is an evident overall decrease of Y - Q characteristic for a very small gap while this characteristic becomes unstable, which is unacceptable. The large gap, which was created as cylindrical, again shows decrease of Y – Q characteristic and in the area of low flows it is on boundary of stability. From obtained results, the original conical gap can be assessed as the best solution of these design variants.

Acknowledgement

The author is grateful for funding and supporting this research to the Grant Agency of Czech Republic under project "Mathematical and Numerical Modeling of Flow in Pipe Junction and its Comparison with Experiment" with registration number 101/09/1539 as well as the junior research grant with sign FSI-J-12-21/1698 and the senior research grant FSI-S-12-2, which are provided by VUT, FSI.

References

Pochylý, F.; Haluza, M.; Drábková, S. (2009) "Stability of Q-Y characteristic of centrifugal pump". *In Engineering Mechanics 2009 – book of extended abstract, Svratka, Czech Republic, May 11-14, 2009*, ISBN 978-80-86246-35-2, pp. 989-996.

Pochylý, F.; Haluza, M.; Klas, R. (2009) "The stability of Y(Q) characteristic curve*". IAHR Symposium on Hydraulic Machinery and Systems, Timisoara, Romania, September 20-24, 2010*, pp. 1-6.

Feranec, M. (200?) *Aplikácie čerpadiel system Turo na čerpanie znečistených kvapalín*. Olomouc: Sigma - výzkumný ústav.

Gančo, M. (1999) *Axiálna sila hydrodynamických čerpadiel s radiálnym obežným kolesom*. Bratislava: Slovenská technická univerzita v Bratislavě.

Egger, Emile & Cie SA. (2008) *Turo vortex pumps* [online]. Egger. Available at WWW: http://www.eggerpumps.com/index.php?id=6&L=2.